ROYAL SOCIETY OF CHEMISTRY

www.rsc.org/crystengcomm

Topochemical Conversion of Protonated Titanate Single Crystal into Platelike $Ba_{0.5}Sr_{0.5}TiO_3$ Mesocrystals with Controllable Microstructures[†]

Dengwei Hu,[†,‡] Xin Luo,[‡] Xingang Kong,[§] Yan Wang,[†] Yasuhiro Tanaka,[‡] and Qi Feng∗,[‡]

[†] *Department of Chemistry and Chemical Engineering, Baoji University of Arts and Science, 1 Gaoxin Road, Baoji, Shaanxi, 721013 PR China*

[‡] *Department of Advanced Materials Science, Faculty of Engineering, Kagawa University, 2217-20 Hayashi-cho, Takamatsu-shi, 761-0396 Japan*

[§] *School of Materials Science and Engineering, Shaanxi University of Science and Technology, Weiyang, Xi'an, Shaanxi, 710021 PR China*

∗ Corresponding author. E-mail: feng@eng.kagawa-u.ac.jp; Fax: +81 (0)87-864-2402; Tel: +81 (0)87-864-2402

Abstract

This report introduces a platelike $Ba_{0.5}Sr_{0.5}TiO_3$ (BST) mesocrystal synthesized by a two-step solvothermal soft chemical process. In the first step, a platelike layered titanate $H_{1.07}Ti_{1.73}\square_{0.27}O_4 \cdot xH_2O$ ($\square$: vacancy of Ti) (HTO) single crystal is treated in a $Ba(OH)_2$ solution to obtain a platelike $BaTiO_3$ (BT)/HTO/anatase nanocomposite. In the second step, the generated BT/HTO/anatase nanocomposite is treated in a $Sr(OH)_2$ solution to obtain the platelike BST mesocrystal. The formation mechanism and nanostructure of the mesocrystal are investigated by XRD, TEM, SAED, and FESEM. The platelike BST mesocrystal is constructed from [110]-oriented BST nanocrystals and shows a set of single-crystal-like electron diffraction spots. The mesocrystal is formed via an *in situ* topochemical mesocrystal conversion mechanism. There is a definite relationship between the crystal-axis directions of the HTO precursor and the BTS mesocrystal. The platelike BST mesocrystals with uniform microstructure and high crystallinity can be achieved by controlling ethanol content in the reaction solvent.

1. Introduction

Ordered alignment of nanocrystals into polycrystals constructed from oriented nanocrystals by bottom-up approaches opens up the possibilities of fabricating new materials and devices, which is one of the key topics of modern materials science. [1] The obtained assemblies not only have properties based on the individual nanocrystals, but also exhibit unique collective properties and advanced tunable functions. [2, 3, 4, 5] Mesocrystal, a new class of material, is a polycrystal constructed from well-aligned oriented crystalline nanocrystals. [6] It can be obtained normally via ordered self-assembly or directed assembly approach. [5] The mesocrystals have increasingly become a hot interdisciplinary research area in recent decade owing to their potential applications to catalysis, sensing, and energy storage and conversion. [6, 7, 8, 9, 10, 11]

Up to now, only a handful of investigations on the titanate mesocrystals have been reported, such as $BaTiO_3$ (BT)[12], $SrTiO_3$ (ST),[13, 14, 15] $BaTiO_3/SrTiO_3$ (BT/ST),[16] and the application studies on the titanate mesocrystals are little-known. We have reported some titanate mesocrystals synthesized by solvothermal soft chemical process in our previous works. [17, 18, 19, 20] Very recently, we have reported a successful synthesis of $Bi_{0.5}Na_{0.5}TiO_3$ (BNT) mesocrystal by solid state reaction, [21] and application of the formation mechanism to the fabrication of a [100]-oriented BNT ceramic with high density, high degree of the orientation, and small grain, which shows a larger piezoelectric constant than non-oriented BNT ceramics.[22] This result preliminarily proves that the mesocrystals have a potential application prospect in ferroelectric material field.[16]

In the last decade, the development of the strontium doped nanocrystalline BT derivatives ($Ba_{1-x}Sr_xTiO_3$, BST) has become popular.[23, 24, 25, 26, 27, 28, 29, 30] This is due to that BST

materials show the high dielectric constant combined with a low dissipation factor, which makes BST as one of the promising candidates of dielectric materials for potential applications in tunable microwave devices[31], pyroelectric sensors[32], and dynamic random access memory (DRAM). [33,34] To fabricate further high-performance ferroelectric materials, the simultaneous applications of the oriented engineering and the domain engineering are expected, where an oriented ceramic with high degree of the orientation and small grain is necessary.[22] The utilization of the mesocrystals to develop oriented engineering and domain engineering is very promising to substantially enhance the performance of ferroelectric materials. The mesocrystals with platelike or fibrous morphology can be used as the template for the fabrication of oriented ceramic with high degree of the orientation and small grain by template grain growth (TGG) method.[19] However, the platelike BST mesocrystal has not been reported owing to that it is very difficult to be prepared due to its high orientation, nanoscale, high aspect ratio of two-dimension, and chemical composition of two components.

In this study, we describe a challenge on the synthesis of a platelike BST mesocrystal by a two-step solvothermal soft chemical process based on an *in situ* topochemical mesocrystal conversion mechanism from a platelike layered titanate single crystal precursor for the first time. The obtained platelike BST mesocrystal is a polycrystal constructed from uniform crystal-axis-oriented BST nanocrystals which show a set of single-crystal-like electron diffraction spots. The [100], [001], and [010] crystal-axis-directions of the layered titanate single crystal correspond to the [001], [1-10], and [110] directions of the BST mesocrystal, respectively. We focus on synthesis of $Ba_{0.5}Sr_{0.5}TiO_3$ mesocrystal because its synthesis process can be easily

applied to the syntheses of a series of $Ba_{1-x}Sr_xTiO_3$ continuous solid solution mesocrystals.

2. Experimental section

All reagents used in this study were of analytical grade and without further purification. Platelike $H_{1.07}Ti_{1.73}\square_{0.27}O_4 \cdot xH_2O$ ($\square$: vacancy of Ti) (HTO) single crystals were prepared as reported by us previously.[35] For the synthesis of the platelike BST mesocrystal, firstly an one-step solvothermal process by solvothermal treatment of HTO-Ba(OH)$_2$-Sr(OH)$_2$ mixture was carried out. BST single phase cannot be obtained but a mixture of a new layered titanate, $Ba_{0.67}Sr_{0.33}TiO_3$, and anatase (Fig. S1). Therefore, we designed an ingenious two-step solvothermal soft chemistry process to synthesize the platelike BST mesocrystal. In the first step, the platelike HTO crystals (0.096 g) were partially reacted with Ba(OH)$_2$ (molar ratio of Ti/Ba = 2) in 30 mL water-ethanol mixed solvents with different volume ratios under solvothermal and stirring conditions at 150 °C for 12 h, respectively. After washing the obtained sample with 0.1 mol·L^{-1} acetic acid and distilled water in sequence, the first-step product was obtained. In the second step, the first-step product sample (0.094 g) was solvothermally treated with Sr(OH)$_2$ (0.114g Sr(OH)$_2 \cdot 8H_2O$, Sr/Ti mole ratio = 0.75:1 in the reaction system) in 30 mL water-ethanol mixed solvents with different volume ratios under stirring condition at 200 °C for 12 h. After the second-step solvothermal treatment, the product was filtered firstly, and then washed with 0.1 mol·L^{-1} acetic acid and distilled water in sequence, finally dried at room temperature.

The structures of crystalline samples were investigated using a powder X-ray diffractometer (Shimadzu, XRD-6100) with Cu Kα (λ = 0.15418 nm) radiation. The

size and morphology of the samples were observed using field emission scanning electron microscopy (FESEM) (Hitachi, S-900) or scanning electron microscopy (SEM) (JEOL, JSM-5500S). Transmission electron microscopy (TEM) and high-resolution TEM (HRTEM) observations, and selected-area electron diffraction (SAED) were performed on a JEOL Model JEM-3010 system at 300 kV, where the samples were supported on a Cu microgrid. Energy-dispersive spectroscopy (EDS; JEOL JED-2300T) was measured also on the TEM system.

3. Results and discussion

Fig. 1 shows the XRD patterns and the FESEM images of the HTO crystals before and after solvothermal treatments with $Ba(OH)_2$ in water solvent and water-ethanol mixed solvent with a volume ratio of 5:25 at 150 °C for 12 h. Before the solvothermal treatment, the basal spacing of 0.882 nm corresponds to the (020) crystal plane of HTO crystal with a layered lepidocrocite (γ–FeOOH)-type structure (Fig. 1A-a).[36] HTO crystal shows a typical platelike morphology with smooth surface (Fig. 1B-a). After treatment in water solvent, small particles with an average size of about 10 nm are sparsely distributed on the surface of the platelike particles (Fig. 1B-b). After the treatment in water-ethanol mixed solvent, the platelike particle surface is densely covered by small particles with an average size of about 50 nm (Fig. 1B-c). The unreacted HTO and generated BT phases can be easily observed after the treatments under the different conditions (Fig. 1A-b, c), indicating that the HTO precursor is partially transformed to BT phase. The BT phase can be well identified by JCPDS File No. 71-1964 (cubic symmetry). The crystal structure of BT polymorph is tetragonal symmetry at room temperature usually. The formed BT phase can be indexed to a pseudocubic unit cell because of small tetragonal distortion. The basal

6

spacing of the unreacted HTO crystal decreased to 0.868 nm due to H^+/Ba^{2+} ion-exchange in the layered structure. These results reveal that the platelike morphology can be maintained and the mixed phases of BT and HTO can be obtained under the solvothermal conditions at 150 ^{o}C.

To further understand the formation of the mixed phases of BT and HTO from HTO single crystal in detail, TEM/HRTEM observations and SAED investigations of the HTO crystals before and after the solvothermal treatment were performed. In the SAED pattern of HTO, the clear and ordered diffraction spots can be easily assigned to the HTO phase with orthorhombic system located along the [010] zone axis (Fig. S2b). The [010] direction (*b*-axis direction) is perpendicular to the basal plane of the platelike HTO crystal. Fig. 2 shows TEM images and SAED patterns of the HTO crystals after the solvothermal treatments with $Ba(OH)_2$ in different solvents. The TEM images of the samples obtained in water and water-ethanol mixed solvent show the platelike morphology and different microstructures on the surface of platelike crystals, which are consistent with the FESEM images (Fig. 1B-b, c), respectively. In the SAED patterns of Fig. 2b and d, three sets of SAED spots for the layered HTO lepidocrocite phase, the BT perovskite phase, and slight anatase phase are simultaneously observed in one platelike crystal, revealing that BT, HTO, and anatase phases coexist in one platelike crystal. The [100] and [001] directions of the HTO phase correspond to the [001] and [1-10] directions of the BT phase, and to the [100] and [001] directions of the anatase phase, respectively. The anatase phase can be formed because of dehydration of HTO crystal under solvothermal treatment conditions. The anatase phase cannot be observed in the XRD patterns (Fig. 1A-b, c) due to its very low crystallinity. These results suggest that the platelike BT/HTO/anatase nanocomposites can be obtained by solvothermal treatment of HTO

in $Ba(OH)_2$ solutions. The obtained samples are designated as BHA-x/y, where x/y is volume ratio of water/ethanol.

It can be confirmed that the crystalline phase of small nanoparticles locating on the platelike particle surface in BHA-30/0 sample is same as the platelike particle rather than the BT single phase (see Fig. S3). This result reveals that the small nanoparticles locating on the platelike particle surface are derived from the broken platelike BT/HTO/anatase particles. The dominant lattice fringe of 0.201 nm in HRTEM image of the platelike particle can be assigned to for the (002) plane of the BT phase (Fig. 2e), suggesting that the surface of BHA-5/25 sample obtained in water-ethanol mixed solvent is constructed mainly from BT nanocrystals. The direction of the (002) plane of the BT phase agrees with the SAED pattern in Fig. 2d. Multi-sets of lattice spots (Fig. 2f) indicate that multi-phases (BT, HTO, and anatase) coexist in the selected area and the crystal-axis directions also agree with the SAED patterns in Fig. 2d.

In order to obtain the platelike BST mesocrystal, in the second step, the BT/HTO/anatase nanocomposites were solvothermally treated with $Sr(OH)_2$ in water-ethanol mixed solvent with different volume ratios. Fig. 3A presents the XRD patterns of the samples obtained by the solvothermal treatments of different kinds of platelike BT/HTO/anatase nanocomposites in $Sr(OH)_2$ water solvent and water-ethanol mixed solvent with a volume ratio of 10:20 at 200 °C for 12 h. The shown diffraction lines can be well identified by JCPDS File No. 39-1395 (cubic symmetry) for BST solid solution except Fig. 3A-d. The diffraction peaks in Fig. 3A-d are broader than those of other samples, which is due to the formation of a $Ba_xSr_{1-x}TiO_3$/BT/ST nanocomposite. The full width at half maximum (FWHM) values of (110) peaks of the BST samples in Fig. 3A were estimated from the XRD data as 0.231, 0.532, 0.618, and 0.655 ° for the samples in Fig. 3A-(a) to (d), respectively. This result reveals that

the crystallinity of BST phase increases with increasing the water content in the reaction solvent of the first and second steps of solvothermal treatments. These results suggest that the BST solid solution can be obtained by the solvothermal treatment of the BT/HTO/anatase nanocomposites in $Sr(OH)_2$ solution. The obtained samples are designated as BST-x/y-m/n, where x/y and m/n are volume ratios of water/ethanol in the first and second steps, respectively. The FESEM results indicate that all the samples show the platelike morphology and polycrystal composition (Fig. 3B), suggesting formation of the platelike polycrystalline BST solid solution. The nanocrystals in BST-30/0-30/0 platelike particles have a larger average size (140 nm) than those in BST-5/25-30/0 (54 nm), BST-30/0-10/20 (47 nm), and BST-5/25-10/20 (45 nm) platelike particles. These results agree with the FWHM values of XRD diffraction peaks. These results imply that the nanoparticles grew up after the second step of solvothermal treatment, and nanoparticle size of the BST solid solution can be controlled and restrained by the introduction of ethanol. When the ethanol was introduced into both the first and second steps of solvothermal reactions, the obtained platelike BST polycrystal was constructed from the smallest nanocrystals. This is due to that the reactivities of HTO, BT, BST, and $Sr(OH)_2$ in water-ethanol mixed solvent decrease with increasing ethanol content, owing to decrease of their solubilities, leading to restrain the growth up of the BST nanocrystals.[17,20]

TEM images and SAED patterns of the BST-30/0-30/0 and BST-5/25-10/20 samples are shown in Fig. 4, and the BST-5/25-30/0 and BST-30/0-10/20 samples are also illustrated in Fig. S4. All the obtained samples present the platelike morphology and polycrystal structure constructed from nanocrystals. The constituent nanocrystals with different size distributions in the platelike polycrystals are consistent with the FESEM images in Fig. 3B, respectively. The SAED patterns except Fig. 4d show a set

of single-crystal-like SAED spots which can be assigned to the BST phase with [110]

zone axis located on the basal plane (Fig. 4b, S4b and d), which agree with XRD

patterns in Fig. 3A, respectively. Fig. 4d shows three sets of possible SAED spots

which can be assigned to $Ba_xSr_{1-x}TiO_3$, BT, and ST phases. This result agrees with the

XRD result (Fig. 3A-d), and further confirms that the BST-5/25-10/20 sample is a

$Ba_xSr_{1-x}TiO_3$/BT/ST nanocomposite. The crystal boundary regions between two

primary nanocrystals inside a mesocrystal can be observed in HRTEM images (Fig.

4e and f). In the BST-5/25-30/0 sample, two primary nanocrystals show the same

lattice fringes of 0.279 nm with the same orientation, corresponding to the (1-10)

plane of BST phase, which reveals the platelike polycrystal is constructed from BST

nanocrystals with the same orientation. In the BST-30/0-10/20 sample, however, the

lattice fringes of 0.279 nm, corresponding to the (1-10) plane of the BST phase, and

lattice fringes of 0.276 nm, corresponding to the (1-10) plane of the ST phase, are

observed in two different primary nanocrystals. The BST and ST nanocrystals have

the same orientation. These results are consistent with their SAED patterns in Fig. 4,

respectively. The above results imply that the platelike BST solid solution

polycrystals are mesocrystals. The platelike BST mesocrystals with controllable

microstructures can be prepared by the two-step solvothermal reaction process.

The chemical composition distributions in these platelike mesocrystals are

investigated using EDS analysis. Three positions in each platelike BST-30/0-30/0,

BST-5/25-30/0, BST-30/0-10/20, and BST-5/25-10/20 mesocrystal samples illustrated

in TEM images (Fig. 4a, S4a, S4c, 4c, respectively) show the almost the same EDS

spectra (Fig. S5), suggesting uniform chemical composition distributions of Ba and Sr

in the electron beam size area of about 200 nm in the each platelike BST solid

solution mesocrystal. The molar ratios of Ti:Ba:Sr from EDS analysis results in the

platelike BST solid solution mesocrystals are listed in Table S1. Each investigating position of obtained platelike mesocrystal sample indicates almost same molar ratio of Ti:Ba:Sr, revealing that the component contents are equally distributed. However, the different samples show slightly different Ti:Ba:Sr mole ratios. The average molar ratio of Ti:Ba:Sr in BST-30/0-30/0 sample is close to the stoichiometric composition of 1:0.5:0.5. However, the lacking Ba and Sr are observed in BST-30/0-10/20 and BST-5/25-10/20 samples, because of low crystallinity and lattice defect. These results imply that the BST-30/0-30/0 mesocrystal sample is a more promising candidate for the domain and orientation engineering applications by considering its smaller nanocrystal size and higher crystallinity. [21,37]

Based on the description above, a detailed mesocrystalline conversion process from the HTO single crystal precursor to mesocrystalline BST solid solution and their topological correspondences can be described as a schematic diagram in Fig. 5. In the first step, half of the HTO crystal is transformed to the BT nanocrystals because the Ti/Ba mole ratio in the reaction system is 1/0.5. Initially, Ba^{2+} ions are intercalated into the HTO bulk crystal through its interlayer pathway by an H^+/Ba^{2+} exchange reaction, and then the Ba^{2+} ions react with the TiO_6 octahedral layers of HTO in the bulk crystal to form the BT phase.[38] Simultaneously, the HTO layered structure is also partially transformed into anatase-type TiO_2 structure by a topochemical dehydration reaction under the solvothermal conditions. [39] Therefore, the platelike HTO/BT/anatase nanocomposites formed by this reaction have uniform distributions of BT and anatase nanoparticles in the platelike bulk crystals. In the present case, the topochemical conversion reaction is dominative, owing to the low concentration of $Ba(OH)_2$, but a subordinate dissolution-deposition reaction is also possible on the platelike particle surface. When the reaction is carried out in water-ethanol mixed

solvent, the formation reaction of BT nanoparticles preferentially occurs near the surface of the platelike particle, suggesting the low migration ability of Ba^{2+} ions into the HTO bulk crystal in the low polarity solvent. The lower polarity solvent exhibits weaker solvation ability with Ba^{2+} ions, and therefore such solvated Ba^{2+} ions would exhibit the lower migration ability into the HTO bulk crystal and higher reactivity with HTO at HTO particle surface. There is a definitely corresponding relationship between the crystal-axis directions of the structures of HTO precursor and the products of BT and anatase (Fig. 2b and d), namely all the BT and anatase nanocrystals present the same crystal-axis orientation in the [110]-direction and [010]-direction, respectively, agreeing with the [010]-direction of the HTO matrix crystal in one platelike crystal of the BT/HTO/anatase nanocomposite (Fig. 5b).

In the second step of solvothermal treatment of the BT/HTO/anatase nanocomposite in the $Sr(OH)_2$ solution, a topochemical conversion reaction occurs similar to the first step. In the topochemical conversion reaction, incipiently, the Sr^{2+} ions are intercalated into the residual HTO matrix crystal through the interlayer pathway by an H^+/Sr^{2+} exchange reaction, and then the Sr^{2+} ions react with the unreacted HTO matrix crystal to form the ST nanocrystals until consuming all the HTO phase, and then react with anatase nanocrystals to form the ST nanocrystals. Simultaneously, the ST formed and BT nanocrystals further react together at their interface by an epitaxial dissolution-decomposition reaction, resulting in the topochemical formation of the platelike BST solid solution mesocrystal. In the water-ethanol mixed solvent, the lower reactivity of $Sr(OH)_2$ with BT/HTO/anatase nanocomposite results in the formation of smaller BST nanocrystals with lower crystallinity in the platelike particles of BST-5/25-10/20 sample than those in the water solvent. Furthermore, such lower reactivity also results in the formation of

Ba$_x$Sr$_{1-x}$TiO$_3$/BT/ST nanocomposite instead of simple BST solid solution for BST-5/25-10/20 sample. There is a definitely corresponding relationship between the crystal orientations of the HTO precursor and the generated mesocrystal. The [100], [001], and [010] directions of HTO single crystal precursor correspond to the [001], [1-10], and [110] directions of BST mesocrystal, respectively, and crystal-axis of the BST mesocrystal corresponds to that of BT nanocrystals in the BT/HTO/anatase nanocomposite (Fig. 5b).

On the basis of the mechanism described above, to obtain uniform platelike BST mesocrystal with high crystallinity, firstly the uniform distribution of BT nanocrystals in the HTO/BT/anatase nanocomposite are necessary. In the second step reaction of conversion HTO/BT/anatase to BST solid solution mesocrystal, keeping appropriate reactivity in reaction system is important. Under high reactive conditions, the high crystallinity of BST mesocrystal with less lattice defect can be achieved. The reactivity in the reaction systems can be controlled by changing the polarity of the reaction solvent, namely changing ethanol content in the solvent. We call the formation mechanism of the platelike BST solid solution mesocrystal from the HTO crystal a topochemical mesocrystal conversion mechanism.

4. Conclusions

The platelike BST mesocrystal with controllable microstructures can be synthesized by the two-step solvothermal soft chemical process developed in the present study. The mesocrystal is formed via the *in situ* topochemical mesocrystal conversion mechanism, which leads to that all the BST nanocrystals in one BST mesocrystal exhibit the same crystal-axis-orientation and the single-crystal-like electron diffraction pattern. There is a definite relationship between the crystal-axis directions

of the HTO precursor and the BTS mesocrystal. The platelike BST mesocrystals with uniform microstructure and high crystallinity can be achieved by controlling ethanol content in the reaction solvent.

ASSOCIATED CONTENT

Notes

The authors declare no competing financial interest.

Acknowledgements

Supplementary Information.

Electronic Supplementary Information (ESI) available: partial detailed experimental strategy, powder XRD patterns, TEM/HRTEM images, SAED patterns, and SEM images, EDS spectra of some materials reported, and Table S1 Atom quantity ratio of Ti:Ba:Sr from corresponding EDS spectra. See DOI: 10.xxxx/xxxxxxxxxxx.

References

1 M. Antonietti and G. Ozin, *Chem. Eur. J.,* 2004, **10**, 28–41.

2 L. Luo, J. F. Hui, Q. Y. Yu, Z. C. Zhang, D. W. Jing, P. P. Wang, Y. Yang and X. Wang, *CrystEngComm*, 2012, **14**, 7648–7655

3 D. V. Talapin, J–S. Lee, M. V. Kovalenko and E. V. Shevchenko, *Chem. Rev.,* 2010, **110**, 389–458.

4 Z. Nie, A. Petukhova and E. Kumacheva, *Nat. Nanotech.,* 2010, **5**, 15–25.

5 Z. Fang, L. Y. Long, S. H. Hao, Y. X. Song, T. T. Qiang and B. Y. Geng, *CrystEngComm*, 2014, **16**, 2061–2069.

6 H. Cölfen and M. Antonietti, *Angew. Chem. Int. Ed.,* 2005, **44**, 5576–5591.

7 M. Niederbergera and H. Cölfen, *Phys. Chem. Chem. Phys.,* 2006, **8**, 3271–3287.

8 L. Zhou and P. O'Brien, *Small,* 2008, **4**, 1566–1574.

9 R. Q. Song and H. Cölfen, *Adv. Mater.,* 2010, **12**, 1301–1330.

10 J. F. Ye, W. Liu, J. G. Cai, S. Chen, X. W. Zhao, H. H. Zhou and L. M. Qi, *J. Am. Chem. Soc.,* 2011, **133**, 933–940.

11 Y. Q. Liu, Y. Zhang and J. Wang, *CrystEngComm,* 2014, **16**, 5948–5967.

12 F. Dang, K. Kato, H. Imai, S. Wada, H. Hanedad and M. Kuwabarae, *CrystEngComm,* 2010, **12**, 3441–3444.

13 V. R. Calderone, A. Testino, M. T. Buseaglia, M. Bassoli, C. Bottino, M. Viviani, V. Buseaglia and P. Nanni, *Chem. Mater.,* 2006, **18**, 1627–1633.

14 V. Kalyani, B. S. Vasile, A. Ianculescu, M. T. Buscaglia, V. Buscaglia and P. NanniCryst, *Cryst. Growth Des.,* 2012, **12**, 4450–4456.

15 N. H. Park, Y. F. Wang, W. S. Seo, F. Dang, C. L. Wan and K. Koumoto, *CrystEngComm,* 2013, **15**, 679–685.

16 N. Suzuki, M. B. Zakaria, N. L. Torad, K. C. -W. Wu, Y. Nemoto, M. Imura, M. Osada and Y. Yamauchi, *Chem. Eur. J.,* 2013, **19**, 4446–4450.

17 Q. Feng, M. Hirasawa and K. Yanagisawa, *Chem. Mater.,* 2001, **13**, 290−296.

18 Q. Feng, M. Hirasawa, K. Kajiyoshi and K. Yanagisawa, *J. Am. Ceram. Soc.,* 2005, **88**, 1415−1420.

19 X. G. Kong, Y. Ishikawa, K. Shinagawa and Q. Feng, *J. Am. Ceram. Soc.,* 2011, **94**, 3716−3721.

20 X. G. Kong, D. W. Hu, Y. Ishikawa, Y. Tanaka and Q. Feng, *Chem. Mater.,* 2011, **23**, 3978−3986.

21 D. W. Hu, X. G. Kong, K. Mori, Y. Tanaka, K. Shinagawa and Q. Feng, *Inorg. Chem.,* 2013, **52**, 10542–10551.

22 D. W. Hu, K. Mori, X. G. Kong, K. Shinagawa, S. Wada and Q. Feng, *J. Eur. Ceram. Soc.,* 2014, **34**, 1169–1180.

23 M. Niederberger, G. Garnweitner, N. Pinna and M. Antonietti. *J. Am. Chem. Soc.,* 2004, **126**, 9120–9126.

24 T. Hungría, M. Algueró, A. B. Hungríía, and A. Castro, *Chem. Mater.,* 2005, **17**, 6205–6212.

25 G. Caruntu, R. R. Jr, I. Dumitru and C. J. O'Connor, *J. Mater. Chem.,* 2006, **16**, 752–758.

26 Z. Li and H. Fan, *J. Phys. D: Appl. Phys.*, 2009, **42**, 075415.

27 Z. Li and H. Fan, *J. Appl. Phys.*, 2009, **106**, 054102.

28 Z. R. Wang, X. C. Ren, C. W. Leung, S. Q. Shi and P. K. L. Chan, *J. Mater. Chem. C*, 2013, **1**, 3825–3832.

29 P. Sambyal, A. P. Singh, M. Verma, M. Farukh, B. P. Singh and S. K. Dhawan, *RSC Adv.,* 2014, **4**, 12614–12624.

30 B. L. Liu, J. B. Wang, X. L. Zhong, K. Huang, B. Li, F. Wang, J. Xie and Y. C. Zhou, *RSC Adv.,* 2014, **4**, 24533–24537.

CrystEngComm Accepted Manuscript

31 Q. W. Zhang, J. W. Zhai, B. Shen, H. J. Zhang and X. Yao, *Mater. Res. Bull.,* 2013, 48, 973–

977.

32 K. Bethe and F. Welz, *Mater. Res. Bull.,* 1971, **6**, 209–214.

33 G. B. Alers, R. M. Fleming, Y. H. Wong, B. Dennis, A. Pinczuk, G. Redinbo, R. Urdahl, E.

Ong and Z. Hasan, *Appl. Phys. Lett.,* 1998, **72**, 1308–1310.

34 S. Bandyopadhyay, S. J. Liu, Z. Z. Tang, R. K. Singh and N. Newman, *Acta Mater.,* 2009, **57**,

4935–4947.

35 P. H. Wen, H. Itoh, W. P. Tang and Q. Feng, *Langmuir*, 2007, **23**, 11782–11790.

36 M. Iida, T. Sasaki and M. Watanabe, *Chem. Mater.,* 1998, **10**, 3780–3782.

37 E. Uchaker and G. Z. Cao, *Nano Today,* 2014, **9**, 499–524.

38 Q. Feng, Y. Ishikawa, Y. Makita and Y. Yamamoto, *J. Ceram. Soc. Jpn.,* 2010, **118**, 141–146.

39 C. D. Chen, L. F. Xu, G. A. Sewvandi, T. Kusunose, Y. Tanaka, S. Nakanishi and Q. Feng,

Cryst. Growth Des., 2014, **14**, 5801–5811.

Fig. Captions:

Fig. 1 (A) XRD patterns and (B) FESEM images of (a) HTO crystals and samples obtained by solvothermal treatments of HTO-Ba(OH)$_2$ (molar ratio of Ti/Ba = 2) mixtures in (b) water solvent and (c) water-ethanol mixed solvent (volume ratio = 5:25) at 150 °C for 12 h, respectively.

Fig. 2 (a, c) TEM images and (b, d) SAED patterns of samples obtained by solvothermal treatments of HTO single crystals and Ba(OH)$_2$ (molar ratio of Ti/Ba = 2) in (a, b) water solvent and (c, d) water-ethanol (volume ratio = 5:25) mixed solvent at 150 °C for 12 h, respectively. (e) HRTEM image derived from the (e) white pane in (c) TEM image, and FFT (Fast Fourier Transformation) pattern derived from whole region of (e) HRTEM image.

Fig. 3 (A) XRD patterns (B) FESEM of samples obtained by solvothermal treatments of Sr(OH)$_2$ with (a, c) BHA-30/0 and (b, d) BHA-5/25 nanocomposite samples in (a, b) water solvent and (c, d) water-ethanol mixed solvent (volume ratio = 10:20) at 200 °C for 12 h, respectively.

Fig. 4. (a, c) TEM images, (b, d) SAED patterns, and (e, f) HRTEM images of samples obtained by solvothermal treatments of Sr(OH)$_2$ with (a, b, e) BHA-30/0 and (c, d, f) BHA-5/25 nanocomposite samples in (a, b, e) water solvent and (c, d, f) water-ethanol mixed solvent (volume ratio = 10:20) at 200 °C for 12 h. (e, f) HRTEM images derived from the yellow (e, f) panes in (a, c) TEM images, respectively. Blue

lines in HRTEM images indicate boundary regions between two primary nanocrystals.

Fig. 5 (a) Schematic representation of formation mechanism of platelike $Ba_{0.5}Sr_{0.5}TiO_3$ mesocrystal via two-step topochemical soft solvothermal processes from layered protonated titanate single crystal. (b) Variation of crystal structure from layered lepidocrocite (γ–FeOOH)-type structure to perovskite $Ba_{0.5}Sr_{0.5}TiO_3$ structure via an *in situ* topochemical mesocrystal conversion reaction with a rotated behavior of TiO_6 octahedra.

Textual abstract for the table of contents pages

Mesocrystalline $Ba_{0.5}Sr_{0.5}TiO_3$ platelike polycrystals with controllable microstructures are constructed from well-oriented nanocrystals.
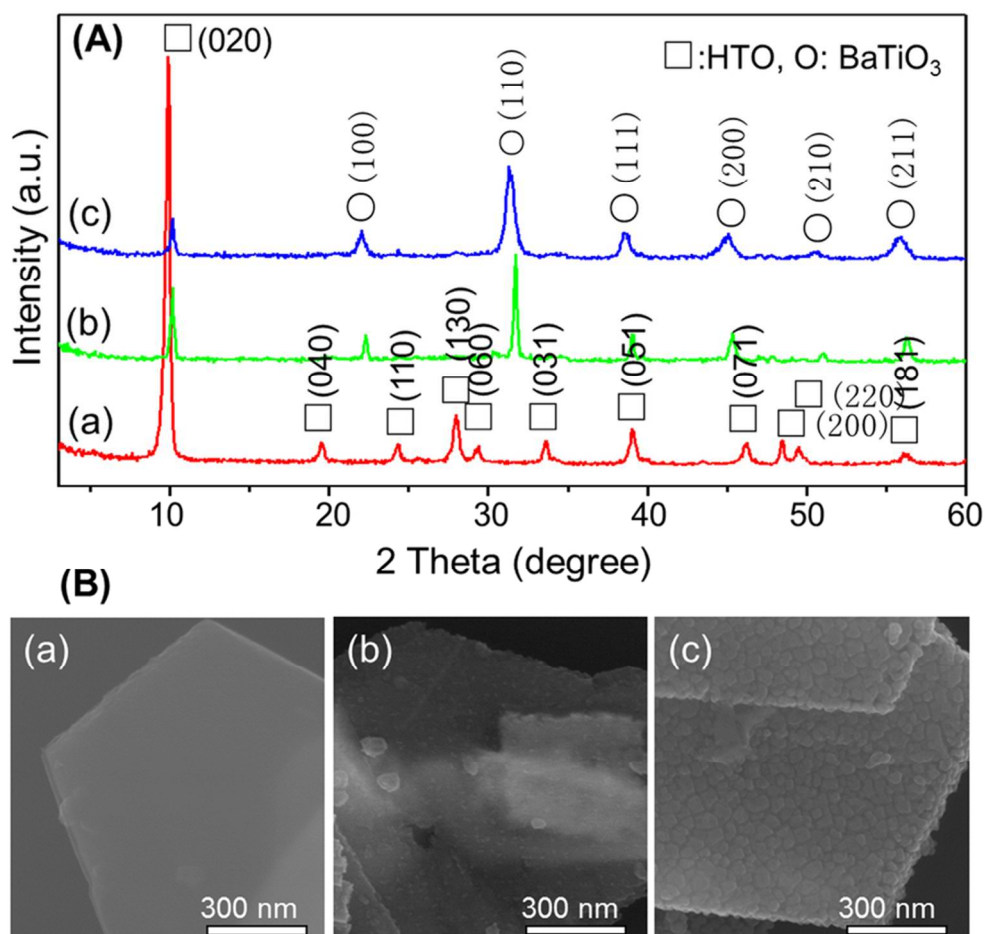
Fig. 1 (A) XRD patterns and (B) FESEM images of (a) HTO crystals and samples obtained by solvothermal treatments of HTO-Ba(OH)2 (molar ratio of Ti/Ba = 2) mixtures in (b) water solvent and (c) water-ethanol mixed solvent (volume ratio = 5:25) at 150 °C for 12 h, respectively.
77x74mm (300 x 300 DPI)
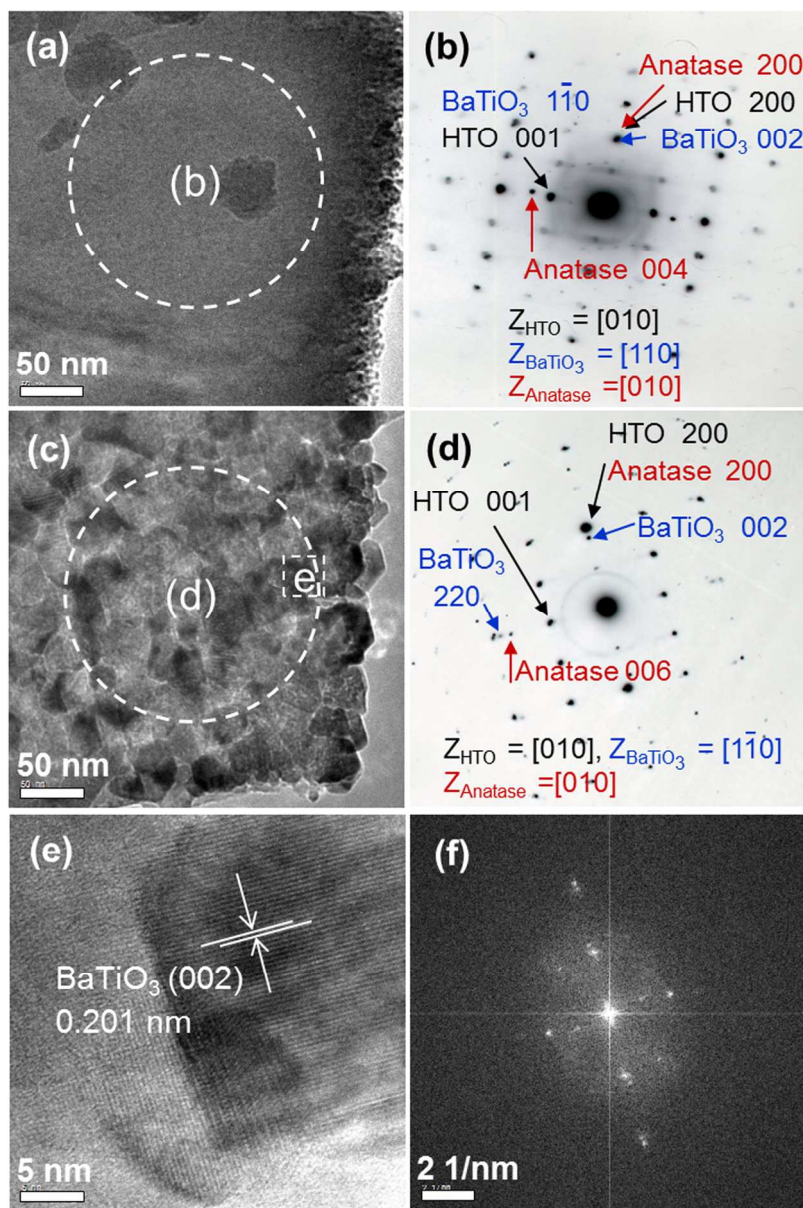
Fig. 2 (a, c) TEM images and (b, d) SAED patterns of samples obtained by solvothermal treatments of HTO single crystals and Ba(OH)2 (molar ratio of Ti/Ba = 2) in (a, b) water solvent and (c, d) water-ethanol (volume ratio = 5:25) mixed solvent at 150 °C for 12 h, respectively. (e) HRTEM image derived from the (e) white pane in (c) TEM image, and FFT (Fast Fourier Transformation) pattern derived from whole region of (e) HRTEM image.
118x175mm (300 x 300 DPI)
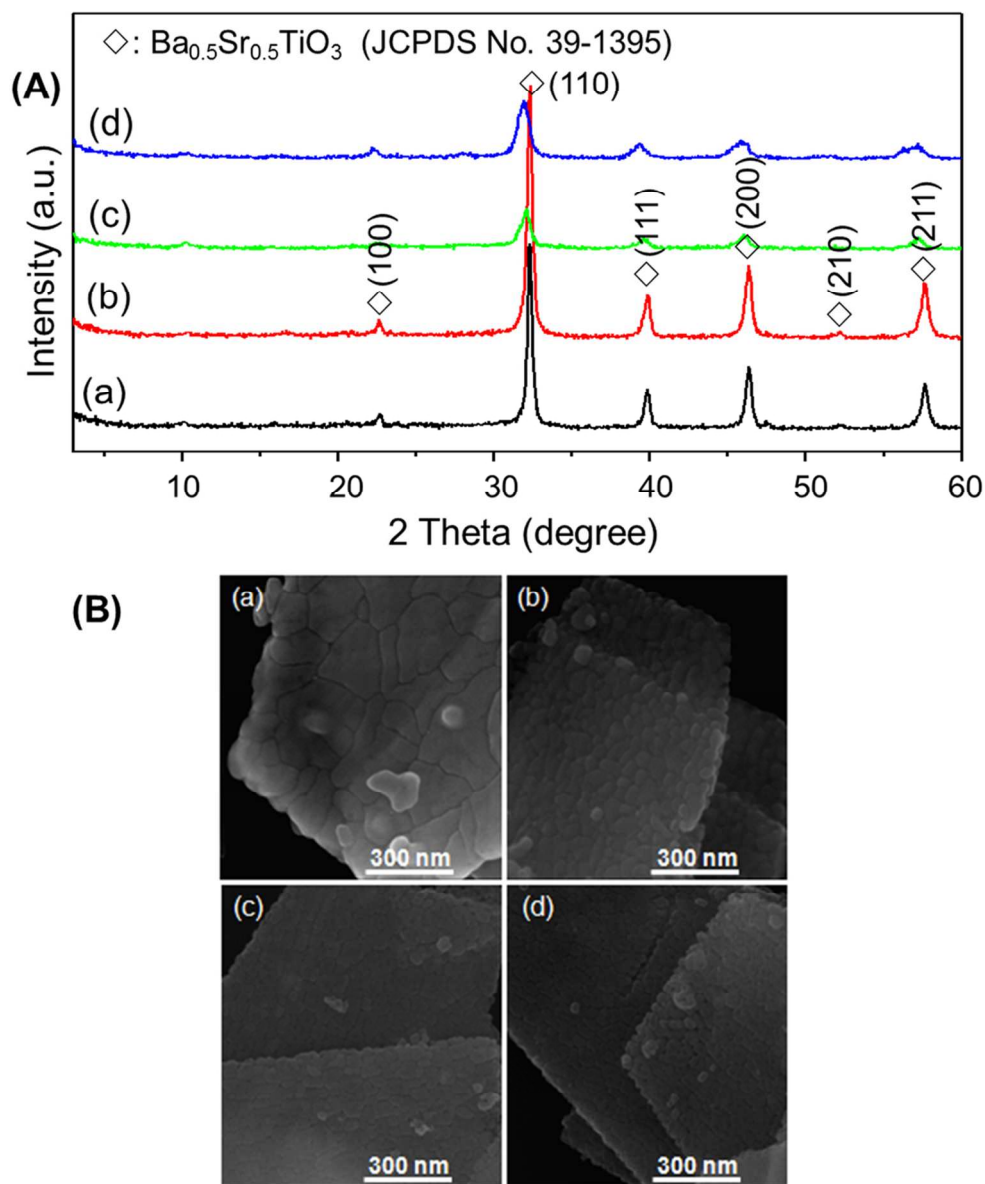
Fig. 3 (A) XRD patterns (B) FESEM of samples obtained by solvothermal treatments of Sr(OH)2 with (a, c) BHA-30/0 and (b, d) BHA-5/25 nanocomposite samples in (a, b) water solvent and (c, d) water-ethanol mixed solvent (volume ratio = 10:20) at 200 °C for 12 h, respectively.
96x115mm (300 x 300 DPI)
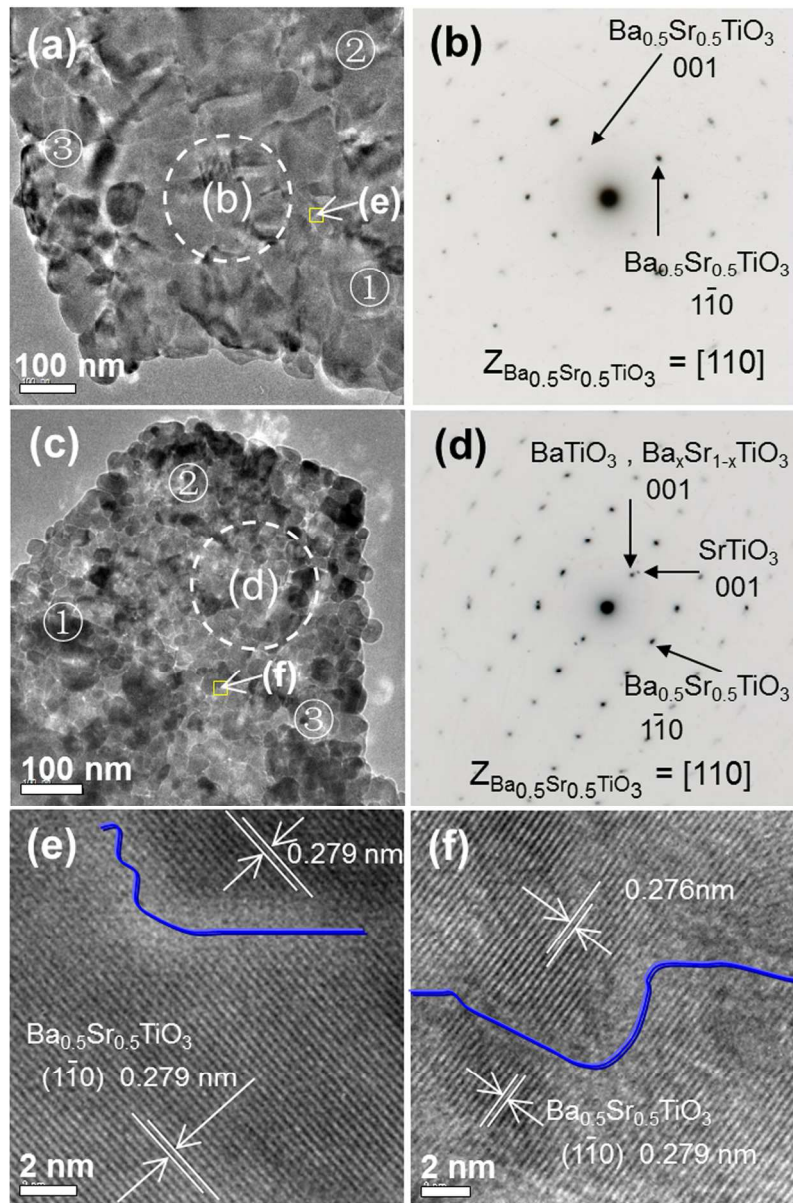
Fig. 4. (a, c) TEM images, (b, d) SAED patterns, and (e, f) HRTEM images of samples obtained by solvothermal treatments of Sr(OH)2 with (a, b, e) BHA-30/0 and (c, d, f) BHA-5/25 nanocomposite samples in (a, b, e) water solvent and (c, d, f) water-ethanol mixed solvent (volume ratio = 10:20) at 200 oC for 12 h. (e, f) HRTEM images derived from the yellow (e, f) panes in (a, c) TEM images, respectively. Blue lines in HRTEM images indicate boundary regions between two primary nanocrystals.
120x181mm (300 x 300 DPI)
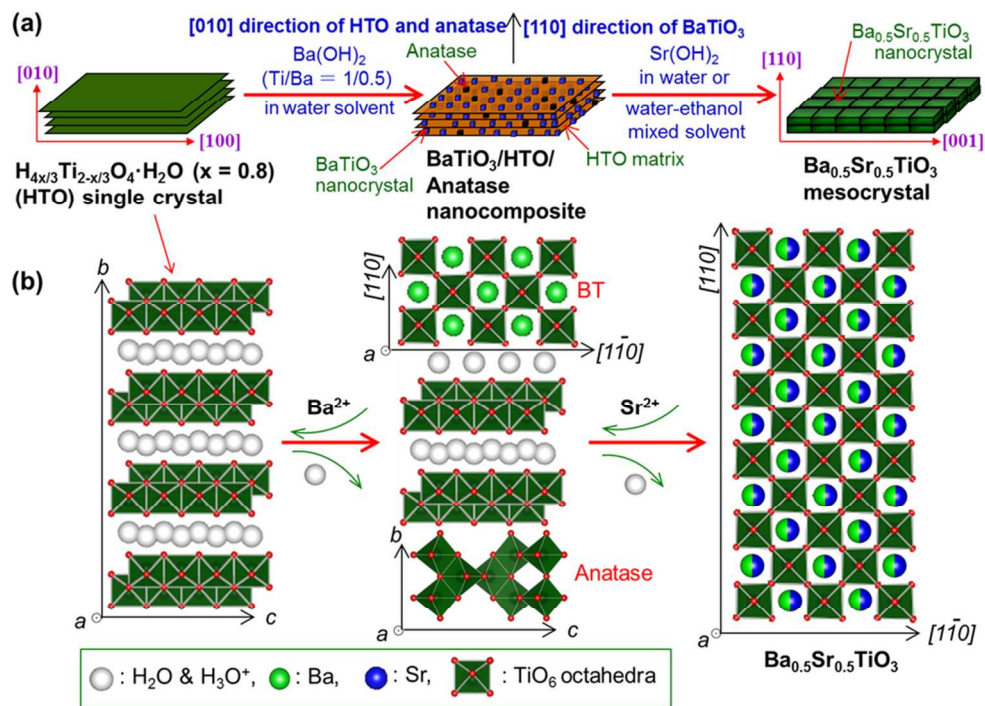
Fig. 5 (a) Schematic representation of formation mechanism of platelike Ba0.5Sr0.5TiO3 mesocrystal via two-step topochemical soft solvothermal processes from layered protonated titanate single crystal. (b) Variation of crystal structure from layered lepidocrocite (γ–FeOOH)-type structure to perovskite Ba0.5Sr0.5TiO3 structure via an in situ topochemical mesocrystal conversion reaction with a rotated behavior of TiO6 octahedra.
85x60mm (300 x 300 DPI)
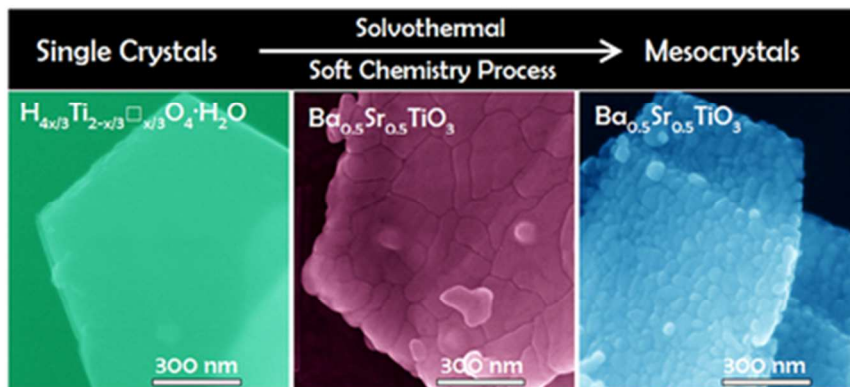
Mesocrystalline Ba0.5Sr0.5TiO3 platelike polycrystals with controllable microstructures are constructed from well-oriented nanocrystals.
36x16mm (300 x 300 DPI)